Inorganic Materials, Vol. 41, No. 7, 2005, pp. 736–742. Translated from Neorganicheskie Materialy, Vol. 41, No. 7, 2005, pp. 841–848.

Phase Equilibria and Crystal Structures of Mixed Oxides in the La–Mn–Ni–O System

A. N. Demina, V. A. Cherepanov, A. N. Petrov, and M. V. Klokova

Gorki State University, pr. Lenina 51, Yekaterinburg, 620083 Russia

e-mail: vladimir.cherepanov@usu.ru

Received October 29, 2004; in final form, January 16, 2005

Abstract—The phase equilibria and crystal structures of mixed oxides in the ternary system La_2O_3–Mn_3O_4–NiO are studied at 1100°C in air. The projection of the La–Mn–Ni–O phase diagram at 1100°C and p_{O_2} = 0.21×10^5 Pa onto the metal-composition triangle is found to comprise 12 phase fields. The lattice parameters of La_2NiO_4 (sp. gr. *I*4/*mmm*), $La_3Ni_2O_7$ (sp. gr. *Cmcm*), $La_4Ni_3O_{10}$ (sp. gr. *Cmca*), and $La_{1+x}Mn_{1-x-y}Ni_yO_3$ solid solutions (sp. gr. *Pnma*, $-0.04 \le x \le 0.05$, $0 \le y \le 0.4$) are determined. The composition stability limits of $La_4Ni_{3-y}Mn_yO_{10}$ solid solutions are $0 < y \le 0.05$. With increasing Ni concentration in $La_{1+x}Mn_{1-x-y}Ni_yO_3$, the metal nonstoichiometry decreases from $-0.04 \le x \le 0.05$ at $y = 0$ to $x = 0$ at $y = 0.4$.

INTRODUCTION

In the past few decades, the unique physicochemical properties of rare-earth 3*d*-transition-metal perovskite oxides (ABO_3) have been the subject of intense research attention. There has been particular interest in A- and B-site substituted manganites with the general formula $La_{1-x}M'_xMn_{1-y}M''_yO_{3\pm\delta}$ (where M' is an alkaline-earth metal, and M'' is a 3*d* transition metal other than Mn), which have been studied most extensively in recent years. Many such manganites have already moved toward the manufacturing stage as materials for fuel cell electrodes [1], magnetoresistors [2], catalysts [3, 4], and other applications. A serious impediment to the optimization of the engineering performance of known manganite materials and the search for new phases for advanced applications is the lack of detailed phase-diagram data for Ln–M'–Mn–M''–O systems.

Phase equilibria in the La–Mn–O, Mn–Ni–O, and La–Ni–O ternaries have been investigated in a number of works. In particular, it has been shown that the stable phase in the La–Mn–O system in air at 1000–1200°C is the perovskite oxide $La_{1\pm x}Mn_{1\pm y}O_{3+\delta}$, which exhibits certain variations in metal and oxygen stoichiometries [5–8]. Under these conditions, the Mn–Ni–O system contains Mn_3O_4- and NiO-based solid solutions: $Mn_{3-x}Ni_xO_4$ ($0 \le x \le 0.06$, hausmannite structure), $Mn_{3-y}Ni_yO_4$ ($0.24 \le y \le 0.81$, spinel structure), and $Ni_{1-z}Mn_zO$ ($0 \le z \le 0.095$) [9]. The La–Ni–O system in air at 1100°C contains three perovskite-like phases: La_2NiO_4, $La_3Ni_2O_7$, and $La_4Ni_3O_{10}$ [10–23]. Two more mixed oxides in this system were obtained under other conditions: $LaNiO_3$ (below 900°C in air or at elevated oxygen pressures [22–26]) and $La_6Ni_5O_{15}$ (at 1200°C in air [20]). Phase-diagram data for the La–Mn–Ni–O system are not available in the literature.

As part of our studies concerned with the phase diagrams of Mn systems (Ln–Mn–O with Ln = Pr, Nd [27], La–Sr–Mn–O [28], La(Sr)–Mn–Cu–O [29], and La(Sr,Ba)–Mn–Co–O [30, 31]), this work focuses on the phase equilibria and structure of mixed oxides in the La–Mn–Ni–O system.

EXPERIMENTAL

Samples for this investigation were synthesized by standard solid-state reactions and by the citrate route. Before synthesis, the starting reagents (LaO-D La_2O_3 and extrapure-grade MnO_2 and NiO) were calcined to remove adsorbed moisture and gases: La_2O_3 at 1200°C for 3 h and NiO at 700°C for 3 h; MnO_2 was heat-treated at 750°C for 3 h in order to convert it to Mn_2O_3, a more stable oxide. Solid-state reactions were conducted in air at temperatures from 850 to 1100°C with intermediate grindings in ethanol every 20 h of firing. The total firing time at 1100°C was 120–200 h. In the citrate process, the starting reagents were dissolved in nitric acid, and crystalline citric acid hydrate powder was added to the resultant solution. Next, the solution was boiled down, and the dry residue was heated from 300 to 800°C with several isothermal holds. In the final step, the samples were fired at 1100°C in air for 96–120 h. All of the samples were quenched by withdrawing the crucibles from the furnace and cooling them on a massive metallic plate.

X-ray diffraction (XRD) examination was performed on DRON-4.0 and DRON-UM1 diffractometers (CuK_α radiation, $2\theta = 20°$–$60°$). Lattice parameters

0020-1685/05/4107-0736

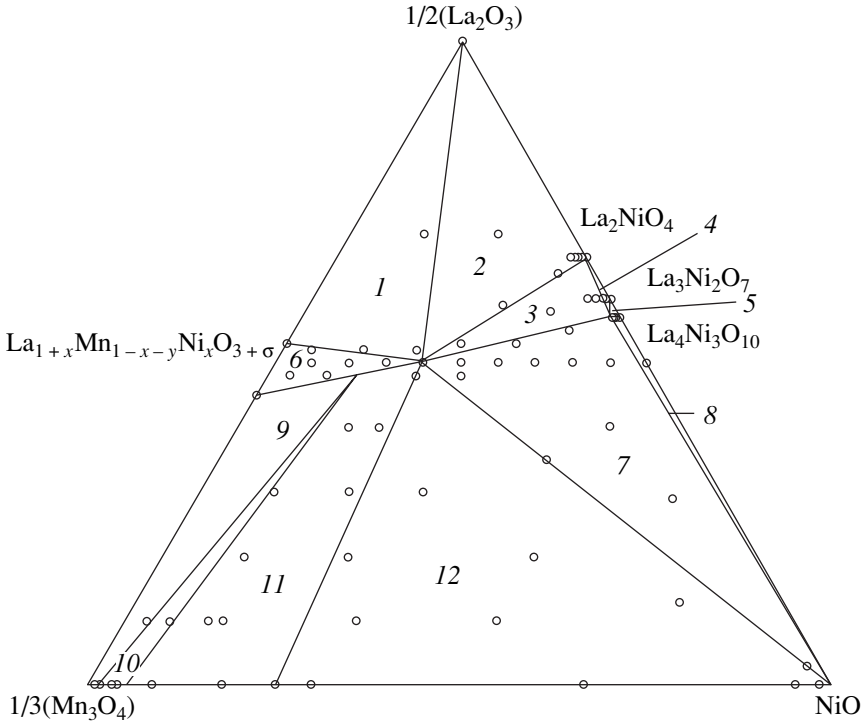

Fig. 1. 1100°C isotherm of the La–Mn–Ni–O system at $p_{O_2} = 0.21 \times 10^5$ Pa projected onto the metal-composition triangle.

were refined using the Rietveld profile analysis method [32].

RESULTS AND DISCUSSION

In our phase-equilibrium studies, we used 70 samples whose compositions are indicated in Fig. 1.

La_2O_3–Mn_3O_4, Mn_3O_4–NiO, and La_2O_3–NiO systems. On the whole, the present results on phase relations in these binary systems agree with earlier data. At the same time, there are some discrepancies. In particular, the $Ni_{1-z}Mn_zO$ solid-solution series ($z \leq 0.05$) reported by Balakirev *et al.* [9] was not detected in the Mn_3O_4–NiO system under the conditions of this study, 1100°C in air, which is probably related to the difference in heat-treatment and quenching conditions.

Our results for the La_2O_3–NiO system confirm the existence of La_2NiO_4, $La_3Ni_2O_7$, and $La_4Ni_3O_{10}$. The structural analysis results for these phases are summarized in Table 1. The phase $La_6Ni_5O_{15}$ [20] was not obtained under the conditions of this study. The XRD pattern from the sample of nominal composition $La_6Ni_5O_{15}$ showed reflections from two phases: $La_4Ni_3O_{10}$ and NiO. Note that Kitayama [20] did not identify $La_6Ni_5O_{15}$ with certainty: it was not obtained in single-phase form, and its XRD pattern is very similar to that of $La_4Ni_3O_{10}$.

La–Mn–Ni–O system. The phase diagram of this quaternary system at constant temperature and pressure can be represented in the form of a tetrahedron. To represent a three-dimensional phase diagram on a plane, binary oxides are often used as components of the system. To obtain a real picture that would represent phases in equilibrium, one must use binary oxides in thermodynamically equilibrium forms under the conditions of interest. The two-dimensional picture thus obtained is in fact a section of the tetrahedron and will only represent the existing intermediate phases if the oxidation states of the three metallic components remain unchanged. In systems containing 3*d* transition metals, including La–Mn–Ni–O, this is rarely, if ever, the case. It is convenient to represent such systems on a plane using a triangle in which compositions are expressed as the mole fractions of the metallic components. The oxygen content of condensed phases cannot then be determined from the phase diagram and is set to be equal to the thermodynamically equilibrium value for each of the coexisting phases. The resulting phase diagram is a projection of the three-dimensional phase relations in the tetrahedron onto the triangle in which compositions are expressed as the mole fractions of the metallic components (for example, $\xi_{Ni} = \frac{n_{Ni}}{n_{La} + n_{Mn} + n_{Ni}}$), and the corners represent the binary oxides $1/2La_2O_3$, $1/3Mn_3O_4$, and NiO in equilibrium at 1000°C in air.

Using XRD data, we constructed a projection of the La–Mn–Ni–O phase diagram at constant temperature

Table 1. Crystal data for mixed oxides in the La_2O_3–Mn_3O_4–NiO system

Phase	Symmetry	Space group	a, Å	b, Å	c, Å	V, Å^3	R_B	R_f
La_2NiO_4	Tetragonal	*I*4/*mmm*	3.862(4)	3.862(4)	12.672(8)	188.97(9)	10.2	5.9
$La_3Ni_2O_7$	Orthorhombic	*Cmcm*	5.392(3)	5.447(2)	20.517(4)	602.61(5)	6.3	5.8
$La_4Ni_3O_{10}$	Orthorhombic	*Cmca*	5.408(5)	5.465(3)	28.037(8)	828.63(2)	4.7	2.6
$La_4Ni_{2.975}Mn_{0.025}O_{10}$	Orthorhombic	*Cmca*	5.737(6)	5.646(6)	21.704(2)	702.99(9)	5.4	3.2
$La_4Ni_{2.95}Mn_{0.05}O_{10}$	Orthorhombic	*Cmca*	5.737(3)	5.645(4)	21.707(6)	702.93(2)	6.1	3.1
$LaMn_{0.9}Ni_{0.1}O_3$	Orthorhombic	*Pnma*	5.533(2)	5.500(5)	7.788(3)	236.99(4)	1.4	1.1
$LaMn_{0.8}Ni_{0.2}O_3$	Orthorhombic	*Pnma*	5.509(1)	5.512(5)	7.796(2)	236.75(3)	0.9	0.8
$LaMn_{0.7}Ni_{0.3}O_3$	Orthorhombic	*Pnma*	5.507(3)	5.501(5)	7.780(2)	235.72(8)	1.2	0.9
$LaMn_{0.6}Ni_{0.4}O_3$	Orthorhombic	*Pnma*	5.476(2)	5.502(8)	7.776(9)	234.27(3)	1.3	1.1
$La_{0.96}Mn_{0.98}Ni_{0.06}O_3$	Orthorhombic	*Pnma*	5.582(6)	5.582(3)	7.793(7)	242.82(5)	1.5	1.5
$La_{1.04}Mn_{0.88}Ni_{0.08}O_3$	Orthorhombic	*Pnma*	5.515(9)	5.498(2)	7.789(9)	236.18(3)	1.8	1.9
$La_{0.96}Mn_{0.88}Ni_{0.16}O_3$	Orthorhombic	*Pnma*	5.511(4)	5.534(9)	7.797(5)	238.05(6)	1.3	1.2

Note: R_B is the Bragg factor, and R_f is the agreement factor.

Table 2. Phase fields in the La_2O_3–Mn_3O_4–NiO system at 1100°C in air

Phase field in Fig. 1	Number of phases	Phase composition
1	2	$La_{1+x}Mn_{1-x-y}Ni_yO_{3\pm\delta}$ ($0 \le x \le 0.05$; $0 \le y \le 0.4$) + La_2O_3
2	3	$LaMn_{0.6}Ni_{0.4}O_3$ + La_2NiO_4 + La_2O_3
3	3	$LaMn_{0.6}Ni_{0.4}O_3$ + La_2NiO_4 + $La_4Ni_{2.95}Mn_{0.05}O_{10}$
4	3	$La_4Ni_{2.95}Mn_{0.05}O_{10}$ + La_2NiO_4 + $La_3Ni_2O_7$
5	2	$La_3Ni_2O_7$ + $La_4Ni_{3-y}Mn_yO_{10}$ ($0 \le y \le 0.05$)
6	1	$La_{1+x}Mn_{1-x-y}Ni_yO_{3\pm\delta}$ ($-0.04 \le x \le 0.05$; $0 \le y \le 0.4$)
7	3	$LaMn_{0.6}Ni_{0.4}O_3$ + $La_4Ni_{2.95}Mn_{0.05}O_{10}$ + NiO
8	2	$La_4Ni_{3-y}Mn_yO_{10}$ ($0 \le y \le 0.05$) + NiO
9	2	$La_{1+x}Mn_{1-x-y}Ni_yO_{3\pm\delta}$ ($-0.04 \le x \le -0.03$, $0 \le y \le 0.18$) + $Mn_{3-z}Ni_zO_4$ ($0 \le z \le 0.015$)**
10	3	Fixed composition $La_{1+x}Mn_{1-x-y}Ni_yO_{3\pm\delta}$*** + $Mn_{2.955}Ni_{0.045}O_4$** + $Mn_{2.89}Ni_{0.11}O_4$*
11	2	$La_{1+x}Mn_{1-x-y}Ni_yO_{3\pm\delta}$ ($-0.03 \le x \le 0$, $0.18 \le y \le 0.4$) + $Mn_{3-z}Ni_zO_4$ ($0.11 \le z \le 0.25$)*
12	3	$LaMn_{0.6}Ni_{0.4}O_3$ + $Mn_{2.75}Ni_{0.25}O_4$* + NiO

* Mn_3O_4-based spinel solid solution.
** Mn_3O_4-based hausmannite solid solution.
*** Approximate composition $La_{0.97}Mn_{0.85}Ni_{0.18}O_{3\pm\delta}$.

and pressure onto the metal-composition triangle (Fig. 1). The phase fields involved are listed in Table 2.

Our results indicate that the degree of Ni substitution for Mn in lanthanum manganite substantially exceeds the degree of Mn substitution for Ni in the lanthanum nickelates. In perovskite oxides based on rare-earth and 3*d* transition metals (Mn–Fe–Co–Ni–Cu), the oxidation state of the 3*d* transition metal decreases systematically. This influences both the stability limits of similar phases and their defect structure. In particular, the average oxidation state of Mn ions in $LaMnO_{3+\delta}$ in air is slightly higher than 3+, that of Co ions in $LaCoO_{3-\delta}$ is slightly lower than 3+, the oxygen-defi-

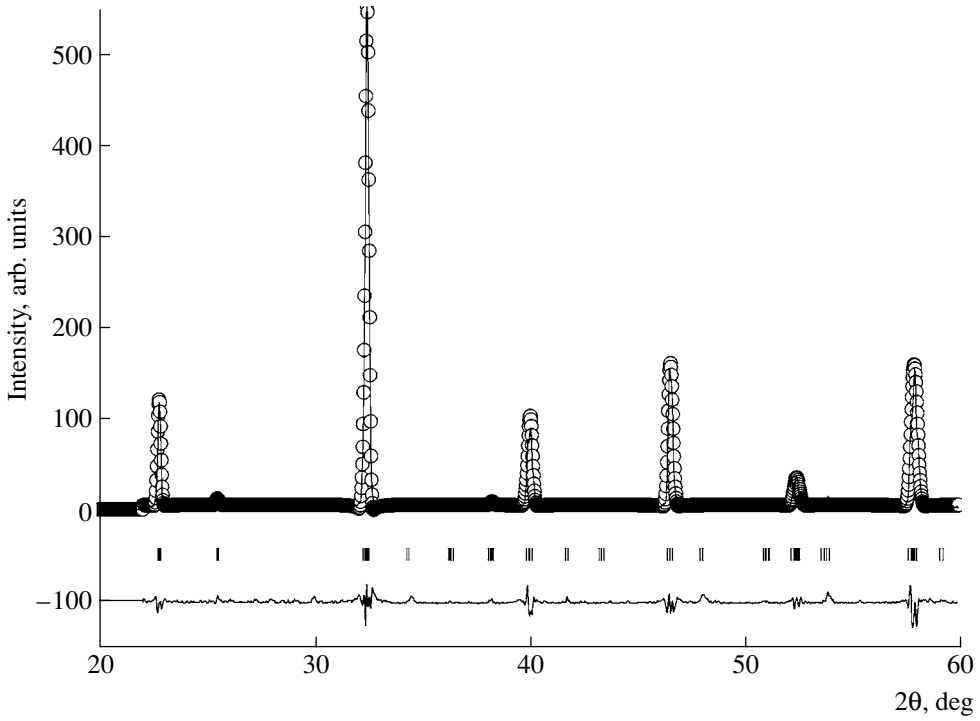

Fig. 2. Rietveld refinement profile for $La_{1.04}Mn_{0.88}Ni_{0.08}O_{3\pm\delta}$.

cient phase $LaNiO_{3-\delta}$ is only stable below 980°C, and the stable phases in air are La_2NiO_4, $La_3Ni_2O_7$, and $La_4Ni_3O_{10}$, in which the average oxidation state of nickel is lower than 3+ [22, 23].

The lability of the oxygen sublattice in the perovskite oxides under consideration plays an important role in determining their physicochemical properties. The possibility of considerable Ni substitution for Mn in $LaMnO_{3+\delta}$ in spite of the marked difference in typical oxidation state between Ni and Mn under identical conditions is attributable to the high mobility of the oxygen sublattice in this manganite. As follows from the electroneutrality condition, charge compensation in nonstoichiometric lanthanum manganite can be represented schematically by the formula $La Mn^{3+}_{1-2\delta} Mn^{4+}_{2\delta} O_{3+\delta}$. After partial nickel substitution for manganese, charge compensation can be represented in the form $LaMn^{3+}_{1-2\delta'-2x} Mn^{4+}_{2\delta'+x} Ni^{2+}_{x} O_{3+\delta'}$. Thus, the superstoichiometric oxygen content δ' decreases with increasing nickel content. A similar width of the homogeneity range was reported by Petrov *et al.* [29] for $LaMn_{1-x}Cu_xO_{3\pm\delta}$. The oxygen content of $LnMn_{1-x}Co_xO_{3\pm\delta}$ (Ln = Pr, Nd) was shown to decrease systematically with increasing Co content [33].

Undoped lanthanum manganite is known to show certain variations in metal and oxygen stoichiometries: $La_{1\pm x}Mn_{1\pm y}O_{3+\delta}$ [5, 8]. With increasing nickel concentration in $La_{1+x}Mn_{1-x-y}Ni_yO_{3+\delta}$, the lanthanum and 3*d*-transition-metal nonstoichiometry decreases from $-0.04 \le x \le 0.05$ at $y = 0$ to zero at $y = 0.4$, and the homogeneity range of the solid solution narrows down to the limiting composition $LaMn_{0.6}Ni_{0.4}O_3$ ($x = 0$). Similar results were obtained for $LaMn_{1-x}Cu_xO_{3\pm\delta}$ [29]. As an illustration, Figs. 2–4 show the XRD patterns of $La_{1.04}Mn_{0.88}Ni_{0.08}O_3$, $La_{0.96}Mn_{0.98}Ni_{0.06}O_3$, and $LaMn_{0.6}Ni_{0.4}O_3$. The structural analysis results for these solid solutions are summarized in Table 1.

Mn substitution for Ni in the lanthanum nickelates is insignificant. In particular, no manganese was detected in La_2NiO_4 and $La_3Ni_2O_7$ to within 2.5 at % accuracy. A slight substitution was revealed in $La_4Ni_3O_{10}$, in which the average oxidation state of nickel must be higher than that in La_2NiO_4 and $La_3Ni_2O_7$. The higher degree of Mn substitution for Ni in $La_4Ni_3O_{10}$ compared to La_2NiO_4 and $La_3Ni_2O_7$ can be understood in terms of their structures. The three phases belong to a homologous series with the general formula $AO(ABO_3)_n$. In the structures of these homologues, every *n* perovskite layers are sandwiched between two AO rock-salt layers. For $La_4Ni_3O_{10}$, $La_3Ni_2O_7$, and La_2NiO_4, $n = 3$, 2, and 1, respectively (Fig. 5). Therefore, $La_4Ni_3O_{10}$ contains layers of oxygen octahedra sandwiched between similar, slightly distorted layers [34], while La_2NiO_4 and $La_3Ni_2O_7$ contain no such layers. In view of this, one would expect an appreciable manganese substitution for nickel in $LaNiO_3$ within its thermodynamic stability region (T, p_{O_2}).

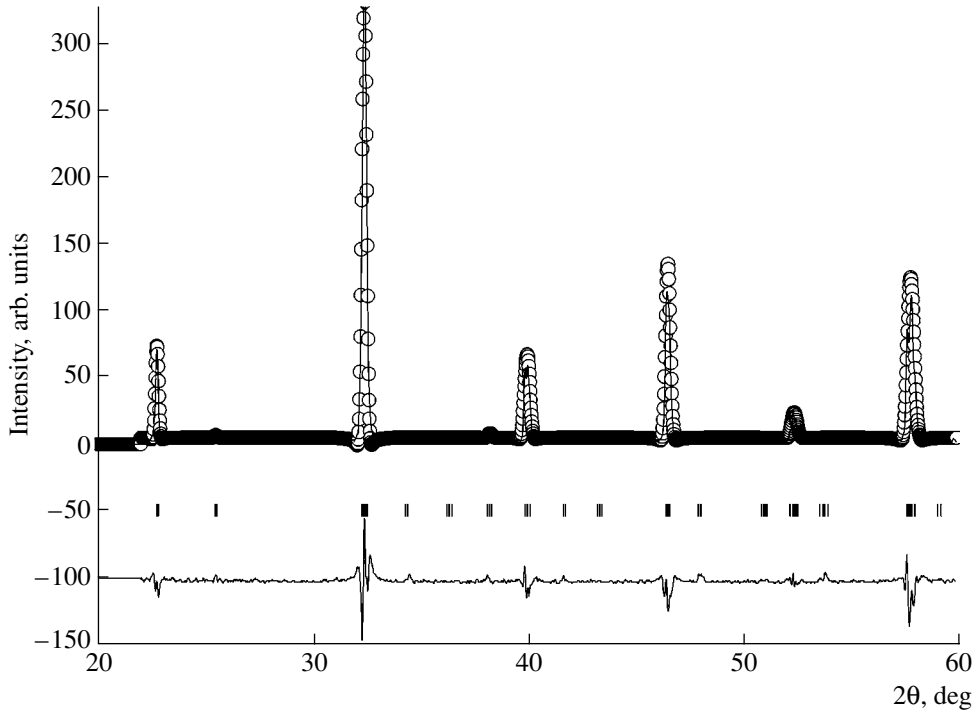

Fig. 3. Rietveld refinement profile for $La_{0.96}Mn_{0.98}Ni_{0.06}O_{3 \pm \delta}$.

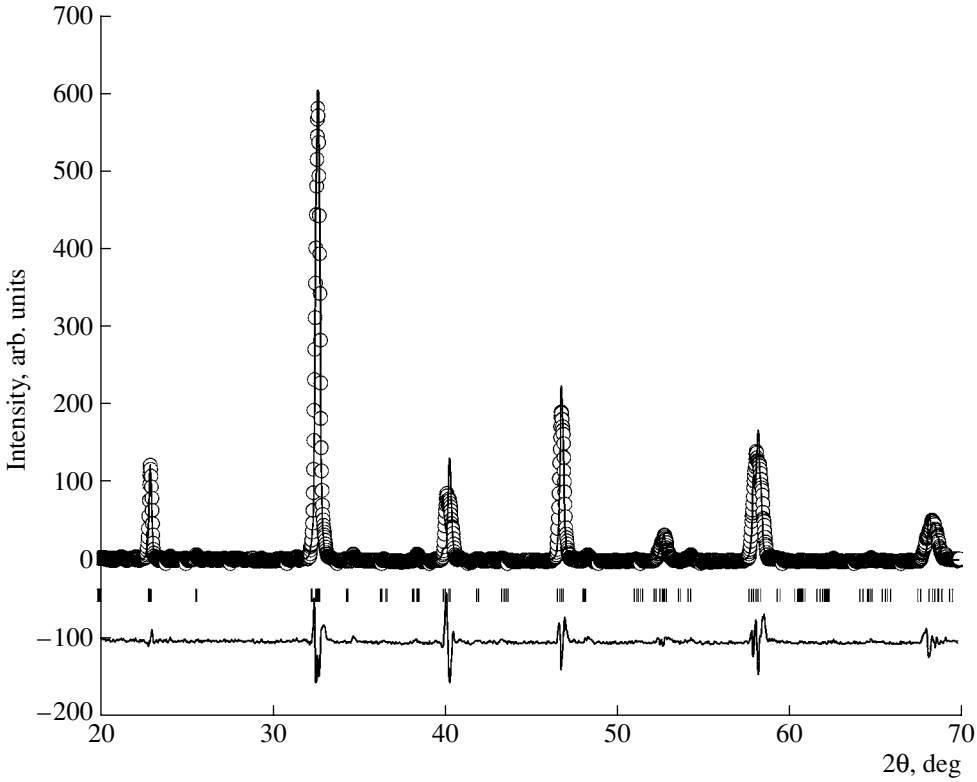

Fig. 4. Rietveld refinement profile for $LaMn_{0.6}Ni_{0.4}O_3$.

To evaluate the homogeneity range of $La_4Ni_{3-y}Mn_yO_{10}$, we prepared (using the citrate process) samples with $0 < y < 0.1$ and $\Delta y = 0.025$. According to XRD data, the homogeneity range of the solid solution in this system is very narrow: $0 < y \le 0.05$. The samples with $y = 0.075$ contained, in addition to the terminal $La_4Ni_{3-y}Mn_yO_{10}$ solid solution, phases with the perovskite and K_2NiF_4 structures.

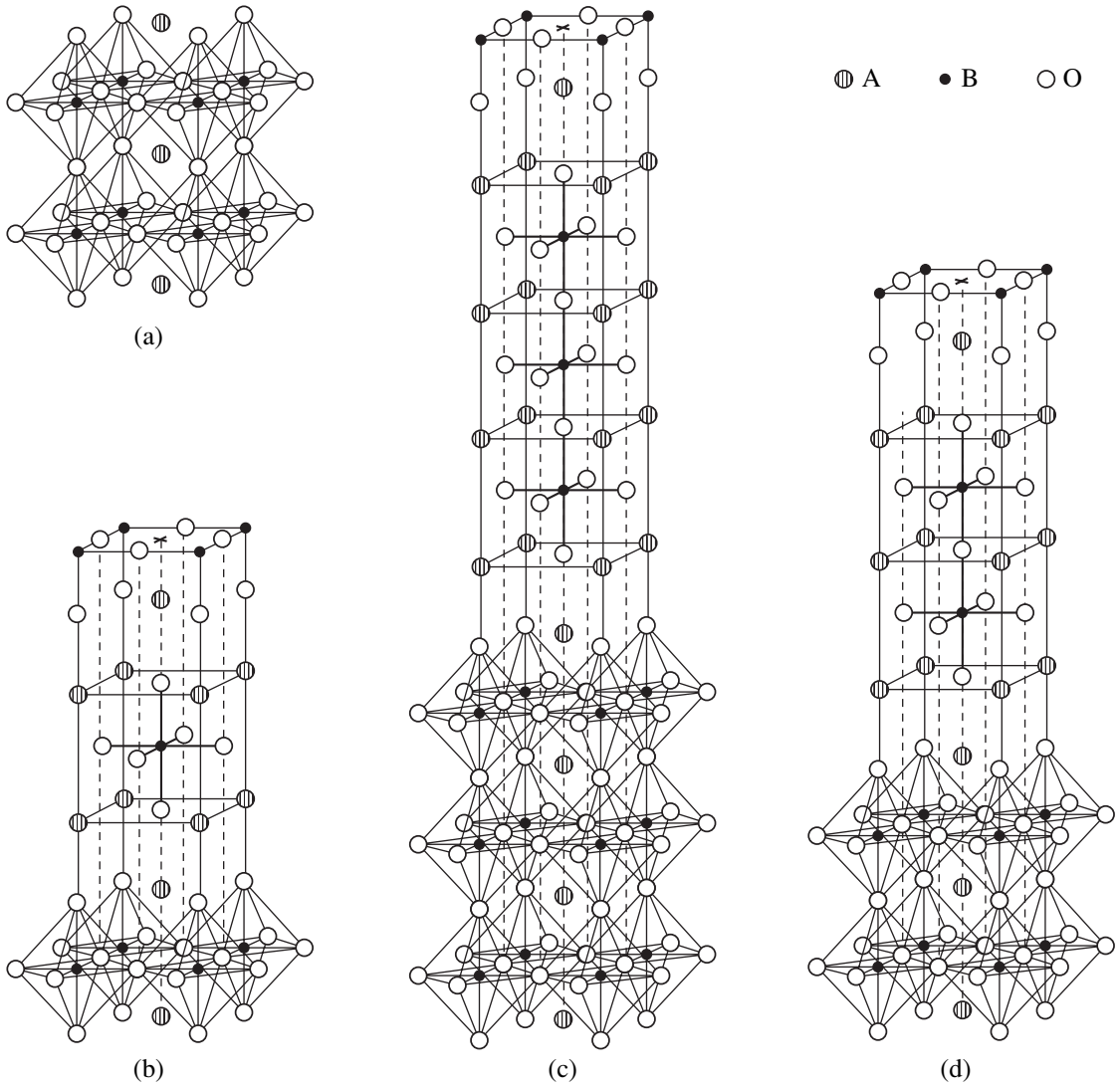

Fig. 5. Crystal structures of $AO(ABO_3)_n$ homologues: (a) $n = \infty$, ABO_3; (b) $n = 1$, A_2BO_4; (c) $n = 3$, $A_4B_3O_{10}$; (d) $n = 2$, $A_3B_2O_7$.

The composition of $La_{1-x}Mn_{1+x-y}Ni_yO_{3+\delta}$ in equilibrium with Mn_3O_4-based hausmannite and spinel solid solutions was estimated using the reported homogeneity range of $Mn_{3-y}Ni_yO_4$ with different structures and the phase compositions of representative points in the composition triangle.

CONCLUSIONS

We constructed a projection of the La–Mn–Ni–O phase diagram at 1100°C and $p_{O_2} = 0.21 \times 10^5$ Pa onto the metal-composition triangle and determined the homogeneity ranges of the solid solutions and the lattice parameters of the mixed oxides in this system.

ACKNOWLEDGMENTS

This work was supported by the Russian Foundation for Basic Research (grant nos. 04-03-96134 and 04-03-32118), the RF Ministry of Education (Basic Research in the Natural Sciences, grant no. E02-5.0-221), and the US Civilian Research & Development Foundation (project REC-005).

REFERENCES

1. Minh, N.Q., Ceramic Fuel Cells, *J. Am. Ceram. Soc.*, 1993, vol. 76, no. 3, pp. 563–588.
2. McCormack, M., Jin, S., Tiefel, T.H., *et al.*, Very Large Magnetoresistance in Perovskite-like La–Ca–Mn–O Thin Films, *Appl. Phys. Lett.*, 1994, vol. 64, no. 22, pp. 3045–3048.
3. Radha, R. and Swamy, C.S., Catalytic Activity of Ln_2MnNiO_6 Perovskites for Isopropanol Decomposition, *Curr. Sci.*, 1983, vol. 52, no. 21, pp. 1012–1013.
4. Kameswari, N., Rajasekhar, B., Radha, R., and Swamy, C.S., Catalytic Decomposition of N_2O on Ln_2MnMO_6 (M = Ni, Cu, and Zn), *Curr. Sci.*, 1985, vol. 54, no. 5, pp. 229–231.

5. Tofield, B.C. and Scott, W.R., Oxidative Nonstoichiometry in Perovskites; an Experimental Survey; the Defect Structure of an Oxidized Lanthanum Manganite by Powder Neutron Diffraction, *J. Solid State Chem.*, 1974, vol. 10, pp. 183–194.
6. Abbatista, F. and Borlera, L., Reduction of $LaMnO_3$: Structural Features of Phases $Ln_8Mn_8O_{23}$ and $Ln_4Mn_4O_{11}$, *Ceram. Int.*, 1981, vol. 7, no. 4, pp. 137–141.
7. Borlera, L. and Abbatista, F., Investigation of the La–Mn–O System, *J. Less-Common Met.*, 1983, no. 92, pp. 55–65.
8. Van Roosmalen, J.A.M., Vlaandheren, P., Cordfunke, E.H.P., *et al.*, Phases in the Perovskite-Type $LaMnO_{3+\delta}$ and the La_2O_3–Mn_2O_3 Phase Diagram, *J. Solid State Chem.*, 1995, vol. 114, pp. 516–523.
9. Balakirev, V.F., Barkhatov, V.P., Golikov, Yu.V., and Maizel', S.G., *Manganity: ravnovesnye i nestabil'nye sostoyaniya* (Manganites: Equilibrium and Metastable Phase Relations), Yekaterinburg, 2000.
10. Rabenau, A. and Eckerlin, F., Die K_2NiF_4 Struktur beum La_2NiO_4, *Acta Crystallogr.*, 1958, vol. 11, no. 4, pp. 304–306.
11. Cherepanov, V.A., Petrov, A.N., and Grimova, L.Yu., Thermodynamic Evaluation of the La–Ni–O System, *Zh. Fiz. Khim.*, 1983, vol. 57, no. 4, pp. 859–863.
12. Petrov, A.N., Cherepanov, V.A., Zuev, A.Yu., and Zhukovsky, V.M., Thermodynamic Stability of Ternary Oxides in Ln–M–O (Ln = La, Pr, Nd; M = Co, Ni, Cu) Systems, *J. Solid State Chem.*, 1988, vol. 77, pp. 1–14.
13. Golub, L.M., Sidorik, L.S., Nedil'ko, S.A., and Fedoruk, T.I., Stability Limits and Some Properties of Rare-Earth Nickelates, *Izv. Akad. Nauk SSSR, Neorg. Mater.*, 1978, vol. 14, no. 10, pp. 1866–1869.
14. Seppanen, M., Crystal Structure of $La_4Ni_3O_{10}$, *Scand. J. Met.*, 1979, vol. 8, pp. 191–192.
15. Kniga, M.V. and Zaretskaya, R.A., Solid-State Phase Relations in the La_2O_3–NiO and Pr_2O_3–NiO Systems, *Izv. Akad. Nauk SSSR, Neorg. Mater.*, 1971, vol. 7, no. 3, pp. 464–467.
16. Drennan, J., Tavares, C.P., and Steele, B.C.H., An Electron Microscope Investigation of Phases in the System La–Ni–O, *Mater. Res. Bull.*, 1982, vol. 17, no. 5, pp. 621–626.
17. Zhang, Z., Greenblatt, M., and Goodenough, J.B., Synthesis, Structure, and Properties of the Layered Perovskite $La_3Ni_2O_{7-\delta}$, *J. Solid State Chem.*, 1994, vol. 108, no. 2, pp. 402–409.
18. Zhang, Z. and Greenblatt, M., Synthesis, Structure, and Properties of $Ln_4Ni_3O_{10-\delta}$ (Ln = La, Pr, and Nd), *J. Solid State Chem.*, 1995, vol. 117, no. 2, pp. 236–246.
19. Carvalho, M.D., Costa, F.M.A., Pereira, I.S., *et al.*, New Preparation Method of $La_{n+1}Ni_nO_{3n+1-\delta}$ (n = 2, 3), *J. Mater. Chem.*, 1997, vol. 7, no. 10, pp. 2107–2111.
20. Kitayama, K., Thermogravimetric Study of the La–Ni–O System, *J. Solid State Chem.*, 1990, vol. 87, pp. 165–172.
21. Mohan, Ram, R.A., Ganapathi, L., Ganguly, P., and Rao, C.N.R., Evolution of Three-Dimensional Character across the $La_{n+1}Ni_nO_{3n+1}$ Homologous Series with Increase in n, *J. Solid State Chem.*, 1986, vol. 63, pp. 139–147.
22. Cherepanov, V.A., Bannikov, D.O., and Safronov, A.P., Thermodynamic Stability of Lanthanum Nickelates, *III Seminar SO RAN–UrO RAN po termodinamike i materialovedeniyu* (III Joint Seminar on Thermodynamics and Materials Research, Sib. and Ural Div., Russ. Acad. Sci.), Novosibirsk, 2003, pp. 51.
23. Bannikov, D.O. and Cherepanov, V.A., Thermodynamical Stability of the Nickel–Lanthanum Complex Oxides, *Z. Anorg. Allg. Chem.*, 2002, vol. 628, no. 9/10, pp. 2180–2182.
24. Wold, A., Post, B., and Banks, E., Rare Earth Nickel Oxides, *J. Am. Chem. Soc.*, 1957, vol. 79, no. 18, pp. 4911–4913.
25. Nakamura, T., Petzow, G., and Gauckler, L.I., Stability of the Perovskite Phase $LaBO_3$ (B = V, Cr, Mn, Fe, Co, Ni) in Reducing Atmosphere: I. Experimental Results, *Mater. Res. Bull.*, 1979, vol. 14, no. 5, pp. 649–659.
26. Demazeau, G., Marbeuf, A., Pouchard, M., and Hagenmuller, P., Sur une série de composés oxygénés du nickel trivalent dérivés de la pérovskite, *J. Solid State Chem.*, 1971, vol. 3, no. 4, pp. 582–589.
27. Cherepanov, V.A., Barhatova, L.Yu., and Petrov, A.N., Phase Equilibrium in the Ln–Mn–O System (Ln = Pr, Nd) and General Aspects of the Stability of the Perovskite Phases, *J. Phys. Chem. Solids*, 1994, vol. 55, no. 3, pp. 229–235.
28. Cherepanov, V.A., Barkhatova, L.Yu., and Voronin, V.I., Phase Equilibria in the La–Sr–Mn–O System, *J. Solid State Chem.*, 1997, vol. 134, no. 1, pp. 38–44.
29. Petrov, A.N., Tikhonova, I.L., and Zuev, A.Yu., Phase Relations in the La(Sr)–Mn–Cu–O Systems and Oxygen Nonstoichiometry of Copper-Substituted Lanthanum Manganates, *Proc.–Electrochem. Soc.*, 1997, vol. 97-40, pp. 927–936.
30. Cherepanov, V.A., Filonova, E.A., Voronin, V.I., *et al.*, Phase Equilibria in the $LaCoO_3$–$LaMnO_3$–$SrCoO_{2.5}$–$SrMnO_3$ System, *Mater. Res. Bull.*, 1999, vol. 34, no. 9, pp. 1481–1489.
31. Cherepanov, V.A., Filonova, E.A., Voronin, V.I., and Berger, I.F., Phase Equilibria in the $LaCoO_3$–$LaMnO_3$–$BaCoO_z$–$BaMnO_3$ System, *J. Solid State Chem.*, 2000, vol. 153, no. 2, pp. 205–211.
32. Rodriges-Carvajal, J., The Programs for Rietveld Refinement, *Physica B* (Amsterdam), 1993, vol. 192, pp. 55–59.
33. Cherepanov, V.A. and Barkhatova, L.Yu., Oxygen Stoichiometry of $LaCo_{1-x}Mn_xO_{3\pm\delta}$ (Ln = Pr, Nd) Solid Solutions, *Neorg. Mater.*, 1998, vol. 34, no. 11, pp. 1314–1317 [*Inorg. Mater.* (Engl. Transl.), vol. 34, no. 11, pp. 1105–1108].
34. Voronin, V.I., Berger, I.F., Cherepanov, V.A., *et al.*, Neutron Diffraction, Synchrotron Radiation, and EXAFS Spectroscopy Study of Crystal Structure Peculiarities of the Lanthanum Nickelates $La_{n+1}Ni_nO_y$ (n = 1, 2, 3), *Nucl. Instrum. Methods Phys. Res., Sect. A*, 2001, vol. 470, pp. 202–209.